SCIENTIFIC REPORTS

OPEN

Fabrication of Stacked MoS_2 Bilayer with Weak Interlayer Coupling by Reduced Graphene Oxide Spacer

Received: 4 February 2019
Accepted: 1 April 2019
Published online: 11 April 2019

Hye Min Oh[1], Hyojung Kim[1], Hyun Kim[1,2] & Mun Seok Jeong[1,2]

We fabricated the stacked bilayer molybdenum disulfide (MoS_2) by using reduced graphene oxide (rGO) as a spacer for increasing the optoelectronic properties of MoS_2. The rGO can decrease the interlayer coupling between the stacked bilayer MoS_2 and retain the direct band gap property of MoS_2. We observed a twofold enhancement of the photoluminescence intensity of the stacked MoS_2 bilayer. In the Raman scattering, we observed that the E^1_{2g} and A_{1g} modes of the stacked bilayer MoS_2 with rGO were further shifted compared to monolayer MoS_2, which is due to the van der Waals (vdW) interaction and the strain effect between the MoS_2 and rGO layers. The findings of this study will expand the applicability of monolayer MoS_2 for high-performance optoelectronic devices by enhancing the optical properties using a vdW spacer.

The recent discovery of a new class of two-dimensional (2D) materials, transition metal dichalcogenides (TMDs), such as molybdenum disulfide (MoS_2) and tungsten disulfide (WS_2), has attracted attention because of their unique layer-dependent electrical and optical properties[1–3]. For example, MoS_2 possesses an indirect band gap of ~1.29 eV in bulk, but it becomes a direct optical band gap of ~1.90 eV in the monolayer and can affect the electronic and optical properties[4,5]. These interesting features in MoS_2 have opened up new possibilities for optoelectronic applications[6]. Previous reports have mainly focused on the fabrication of optoelectronic devices, such as phototransistors, photodetectors, light-emitting diodes, and solar cells with monolayer MoS_2[7–10]. However, the absorbance of monolayer MoS_2 is not strong enough to realize efficient optoelectronic devices[4]. Compared to the monolayer, bilayer or few-layer MoS_2 shows improved absorbance and carrier mobility[11]. However, few-layer MoS_2 has an indirect band gap that limits its applicability for high-efficiency optoelectronic devices. Therefore, many researchers have worked to improve the mobility and intensity of the photoluminescence (PL) of MoS_2 with doping, strain, and defect engineering[12–14]. More recently, it was reported that artificially stacked TMD with a spacer between the individual layers can improve the optical properties while maintaining the intrinsic properties of TMD[15–18]. Among them, Piljae Joo *et al.* demonstrated an enhancement of the photoluminescence (PL) of stacked few-layer MoS_2 with a polymer spacing layer. However, this method has been realized with few-layer or multilayer MoS_2[15]. For the stacking of monolayer TMD, hexagonal boron nitride (h-BN) was introduced as the spacer for the TMD hetero-bilayer or homo-bilayer[16–18]. These results suggest that stacked TMD with the h-BN layer can retain the direct band gap feature of the monolayer TMD. However, the procedure for transferring h-BN onto TMDs is somewhat complicated; thus, it is difficult to apply it to large areas. Therefore, it is essential to devise a simple technique that can be implemented easily into the device-fabrication process to obtain higher optoelectronic properties.

Here, we demonstrate the fabrication of stacked MoS_2 with a reduced graphene oxide (rGO) spacer. rGO has remarkable properties, such as high thermal conductivity, electrical conductivity, and mechanical stability[19]. rGO can decrease the interlayer coupling of stacked MoS_2, such that rGO is an ideal sheet to decouple the top and bottom MoS_2 and retain the direct band gap property of MoS_2. We observed an enhancement of the PL intensity of stacked MoS_2 with an rGO spacer compared to that of monolayer MoS_2. We also systematically investigated the origin the structural, chemical, and optical properties of the stacked MoS_2 with/without spacer layer.

[1]Department of Energy Science, Sungkyunkwan University (SKKU), Suwon, 16419, Republic of Korea. [2]Center for Integrated Nanostructure Physics, Institute for Basic Science (IBS), Suwon, 16419, Republic of Korea. Correspondence and requests for materials should be addressed to M.S.J. (email: mjeong@skku.edu)

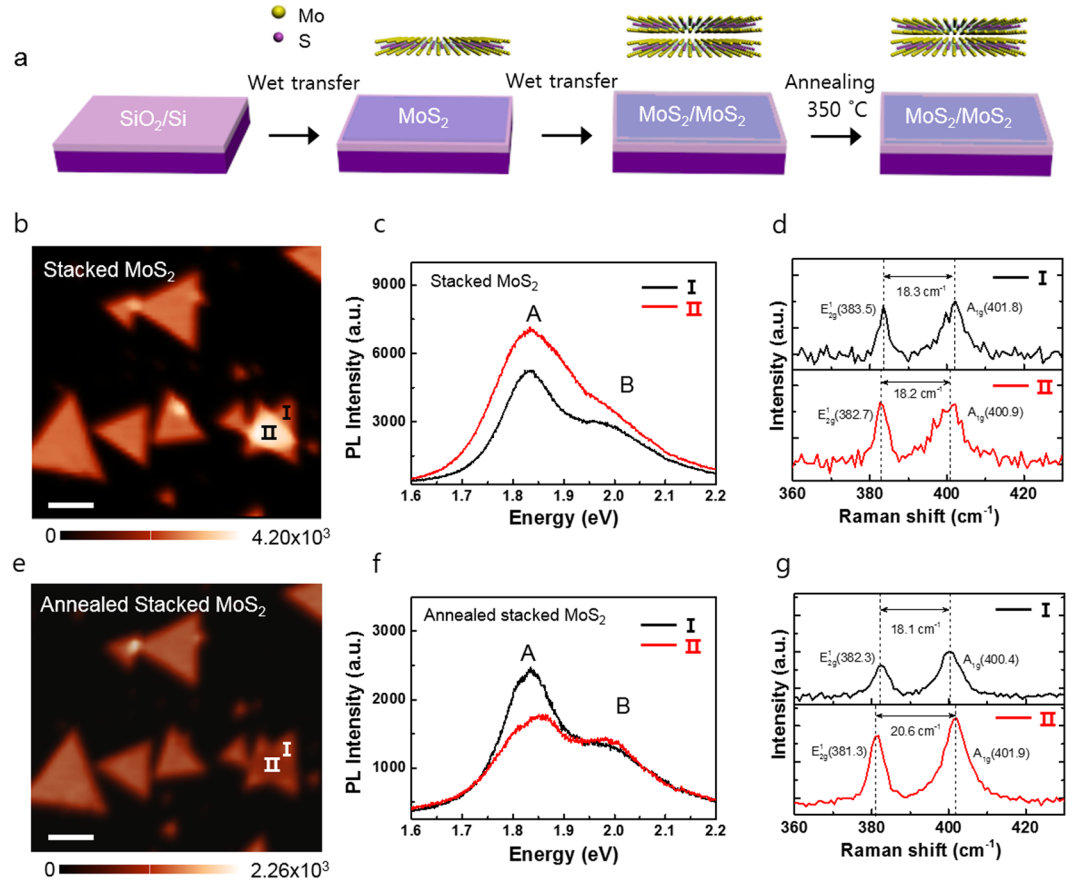

Figure 1. (**a**) schematic of sample preparation of stacked MoS_2 with/without thermal annealing. PL intensity map and PL and Raman spectra of I and II region in the stacked MoS_2 (**b**–**d**) before and (**e**–**g**) after annealing.

Results and Discussion

Figure 1a illustrates the preparation process of stacked MoS_2. The chemical vapor deposition (CVD)-grown monolayer MoS_2 films were transferred onto the 300-nm-thick of SiO_2/Si substrate using the conventional wet transfer method. (See Methods section for details) To prepare stacked bilayer MoS_2, another CVD-grown monolayer MoS_2 film was transferred onto the monolayer-MoS_2/SiO_2/Si template. First, we confirmed the basic optical properties of the monolayer MoS_2 by using the PL and Raman analysis (Supporting Information (SI), Fig. S1). Figure 1b shows the PL intensity map of monolayer MoS_2 flakes and stacked MoS_2 flakes. Normally, the PL intensity of bilayer MoS_2 is much lower than that of monolayer MoS_2 because it has an indirect band gap[4,5].

Interestingly, we observed that the integrated PL intensity of stacked MoS_2 flake (II) is slightly higher than that of the monolayer MoS_2 flake (I). It is implied that stacked bilayer MoS_2 flake has different optical features that are irrelevant to the layer-dependent optical properties of MoS_2.

To confirm the PL peak position of the sample, we extracted the PL spectrum from the stacked MoS_2 flakes marked I and II in Fig. 1b. The A and B exciton peak positions at ~1.83 and ~1.98 eV of I and II were almost the same (Fig. 1c). Figure 1d shows the Raman spectra of I and II. We observed the two Raman modes at approximately 383.5 and 401.8 cm^{-1} of monolayer region I in the stacked MoS_2, corresponding to the E^1_{2g} and A_{1g} modes[20]. The distance between the E^1_{2g} and A_{1g} modes was 18.3 cm^{-1}. The A_{1g} and E^1_{2g} modes of the region II were shifted compared to those of region I, but the distance between the two Raman modes is around 18.2 cm^{-1}, which is related to the monolayer properties of MoS_2[20]. We confirmed the same trend from other stacked MoS_2 flakes, regardless of stacking angle (see SI, Fig. S2). Figure 1e shows the PL intensity map of the same stacked MoS_2 sample after thermal annealing at ~300 °C for 1 h under nitrogen gas. After thermal annealing, the integrated PL intensity was reduced for all of the stacked MoS_2 flakes. The PL intensity of region II is decreased compared to that of region I. In region II of stacked MoS_2, the intensity of exciton peak A decreases significantly and is slightly shifted (Fig. 1f). These PL results show a similar characteristic to the natural bilayer[21,22]. In addition, the distance between the E^1_{2g} and A_{1g} modes increased from ~18.2 to ~20.6 cm^{-1}, which is somewhat similar to the bilayer properties (Fig. 1g)[20]. From the PL and Raman results, we found that annealed stacked MoS_2 regions have bilayer properties.

To investigate the phenomena of the different optical properties of the stacked MoS_2 before and after thermal annealing, we carried out photothermal induced infrared resonance (PTIR) spectroscopy, which simultaneously provides topographical information and infrared absorbance (see SI, Fig. S3)[23]. Fig. 2a,b show the AFM topography images and height profiles of stacked MoS_2 before and after thermal annealing, respectively. The

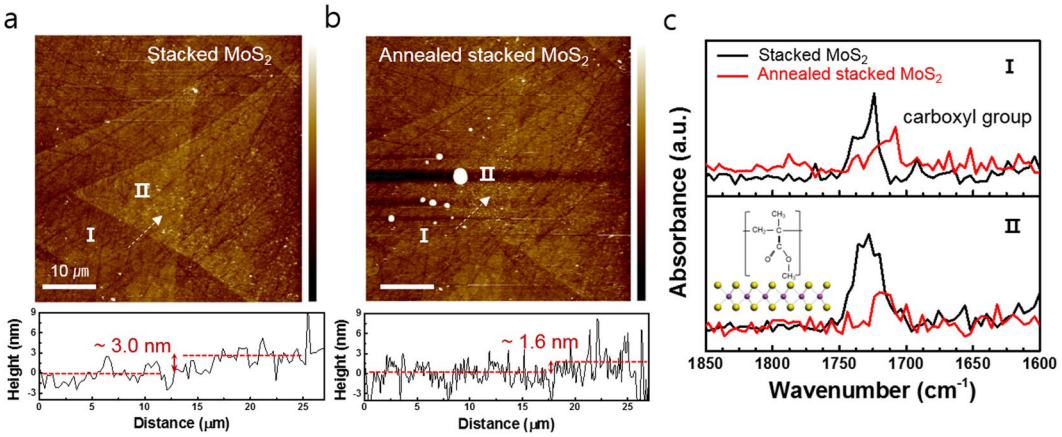

Figure 2. (**a**,**b**) is AFM height image of the stacked bilayer MoS_2 before and after annealing. (**c**) Absorbance spectra of each position of stacked bilayer MoS_2 before and after annealing treatment.

topography images provide distinguishable contrast between the monolayer (I) and stacked (II) MoS_2 region. We measured the thickness of the stacked MoS_2 from region I to II. The thickness of the dashed line at the stacked MoS_2 before thermal annealing was ~3.0 nm. This value is much larger than the expected thickness of the stacked bilayer MoS_2[22]. However, after thermal annealing, the thickness of the stacked MoS_2 decreased to ~1.6 nm, which is almost identical to the thickness of the bilayer MoS_2[22]. According to the previous results, it is assumed that defects or organic molecules exist in between the stacked flakes[21]. Fig. 2c presents the PTIR absorbance spectra of regions I and II of the stacked MoS_2 sample before and after thermal annealing treatment. We observed a peak at approximately 1728 cm^{-1}, corresponding to the C=O mode of the poly(methyl methacrylate) (PMMA) residues on the overall area of the stacked MoS_2 sample before thermal annealing[24]. Normally, PMMA is used as a supporting material during the wet-transfer process. However, polymer residues usually remain on the surface of the TMD thin film after the transfer process, and it is difficult to completely remove them from the TMD thin film[21,25]. Therefore, the stacked bilayer MoS_2 are thicker than the original bilayer MoS_2 because polymer residues are present on MoS_2. The polymer residue suppresses the interlayer interaction between stacked MoS_2 monolayers. Thus, the PL and Raman results of stacked MoS_2 before annealing showed monolayer characteristics (Fig. 1b–d). In contrast, after thermal annealing, the intensity of the C=O mode decreased. This indicates that the concentration of the PMMA is reduced (Fig. 2c). The thermal annealing removed the polymer residues and caused interlayer interaction in stacked MoS_2. Thus, the thickness of stacked MoS_2 decreased after annealing, and it exhibited bilayer characteristics. From these results, the polymer residues between stacked MoS_2 flakes can act as a spacer, which can retain the intrinsic properties of monolayer MoS_2 prior to thermal annealing. However, during the device-fabrication process, the thermal annealing process inevitably decreases the resistivity of the interface for better device performance[26]. Therefore, it is necessary to find the optimum spacer in the stacked MoS_2 that blocks the intercoupling between flakes without damage in the thermal annealing process. Figure 3a shows an illustration of the sample-preparation process of the stacked MoS_2 with spacer layer. The CVD-grown monolayer MoS_2 films were transferred onto the 300-nm SiO_2/Si substrate using the wet-transfer method. The prepared GO solution was spin-coated at 500 rpm for 5 s, followed by 1500 rpm for 60 s on top of the monolayer MoS_2 on the SiO_2/Si substrate. The average thickness of the coated rGO on the MoS_2 sheet was approximately 5 ± 2 nm (see SI, Fig. S4). To prepare hybrid stacked MoS_2, another CVD-grown monolayer MoS_2 film was transferred onto the GO-coated monolayer MoS_2/SiO_2/Si template. By thermal annealing treatment at 350 °C for 3 h, we fabricated the stacked MoS_2 with an rGO spacer. To investigate the reduction of GO, we carried out Raman spectroscopy measurement of the GO before and after thermal annealing (see SI, Fig. S5). Figure 3b is the AFM topography image of the stacked MoS_2 with rGO spacer. According to the AFM topography image, the monolayer and stacked MoS_2 region can be distinguished. Additionally, we observed wrinkles and some bubbles on the stacked MoS_2 with rGO sample. These seems to be formed during the transfer process (see SI, Fig. S6). The thickness of the monolayer MoS_2 with rGO (green dot) is approximately 1.1 nm and that of the stacked bilayer MoS_2 with rGO region (orange dot) is approximately 2.7 nm (see SI, Fig. S7). For the spatially resolved optical characterization, confocal PL and Raman measurements were performed for stacked MoS_2 with rGO spacer. Figure 3c shows the PL spectra obtained from each position of the sample. We observed the A and B excitons (~1.86 and 2.0 eV) of MoS_2 and the Raman G and D bands (~2.13 and 2.16 eV) of the rGO at PL spectra[12]. As shown in Fig. 3c, the PL intensity of stacked bilayer MoS_2 with rGO (M/rGO/M) region is twice that of rGO on monolayer MoS_2 (rGO/M) or monolayer MoS_2 on rGO (M/rGO) regions. In previous reports, PL quenching was observed in MoS_2 over mechanically exfoliated graphene (MEG) because MEG has semi-metallic properties that result in a metal-semiconductor interface[27,28]. On the other hand, rGO show semiconductor behavior because of residual oxygen functional groups after thermal annealing[29,30]. Therefore, PL quenching is not observed in the interface between rGO and MoS_2 stacked structure. Figure 3d represents the PL intensity map for the energy range of 1.67–2.11 eV of stacked bilayer MoS_2 with rGO spacer. The PL intensity map could also be used to distinguish the stacked M/rGO/M, M/rGO, and rGO/M regions because these PL intensity values are different from

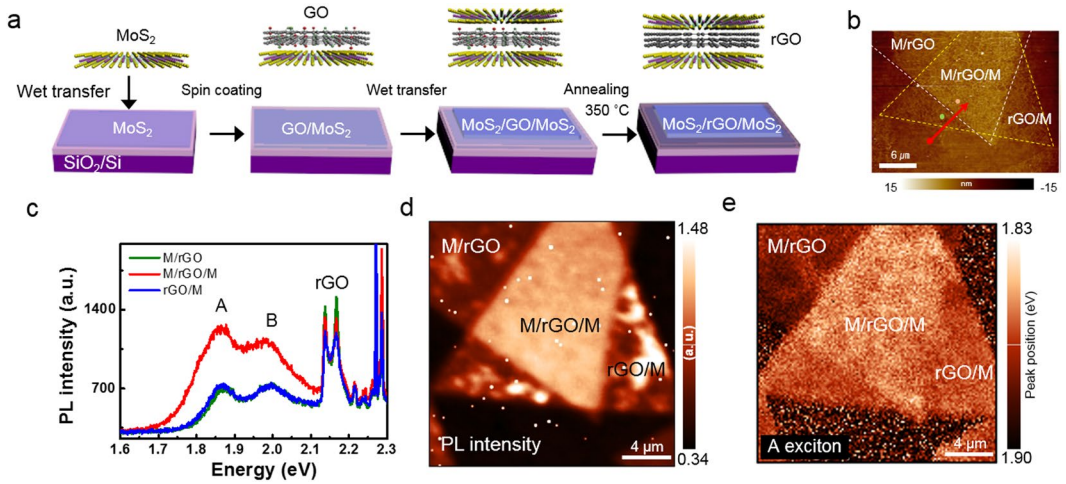

Figure 3. (**a**) Illustration for sample preparation of stacked MoS_2 with rGO. (**b**) AFM topography image of the stacked MoS_2 with rGO. (**c**) PL spectra of the various position of the stacked MoS_2 with rGO. (**d**) PL intensity map image of stacked MoS_2 with rGO for 1.67~2.11 eV corresponding to the MoS_2. (**e**) PL peak position map image of the stacked MoS_2 with rGO.

each other. As observed in Fig. 3d, some position of rGO/M region has a higher PL intensity rather than the M/rGO/M region. To compare the intensity, we extracted the PL spectra of bright spot of rGO/M region and M/rGO/M region (see SI, Fig. S8). According to previous report, GO induce the p-type doping of monolayer MoS_2 because of the functional groups of GO[12]. We believe that the cause of high PL intensity in the rGO/M region is p-type doping by residue of functional group after thermal annealing. A slight red shift in the A exciton peak is observed in the M/rGO/M region. In addition, the PL peak position of the stacked MoS_2 with rGO sample is different (Fig. 3e). We confirmed that the PL results at stacked MoS_2 with rGO spacer showed different characteristics from those of the stacked MoS_2 without rGO spacer.

To clarify the cause for the considerably changed optical and structural properties of stacked MoS_2 with rGO spacer, we have performed confocal Raman mapping. Figure 4a shows the Raman intensity map of the stacked MoS_2 with rGO. The Raman intensity map provides distinguishable contrast between the stacked and monolayer MoS_2 regions. Figure 4b shows the local Raman spectra of each position. The peak positions of the two Raman modes of stacked MoS_2 with rGO spacer are different from those of the stacked MoS_2 without spacer. The A_{1g} and E^1_{2g} modes of stacked MoS_2 with rGO were further shifted compared to those of stacked MoS_2 without spacer. In order to understand these results, we focus on the E^1_{2g} and A_{1g} modes of MoS_2, depending on the region. Figure 4c presents the Raman intensity of the E^1_{2g} and A_{1g} modes of the MoS_2 according to each position. The higher Raman intensity of the M/rGO/M region originates from the increased scattering cross section by stacked MoS_2 with rGO. Figure 4d shows the peak position of the two Raman modes according to the position of the stacked MoS_2 with rGO spacer. The E^1_{2g} and A_{1g} modes of the stacked MoS_2 with rGO spacer were observed to shift to the opposite direction compared to that of pristine monolayer MoS_2 (M). Interestingly, we observed that the red shift of E^1_{2g} on M/rGO/M is large compared to M/rGO and rGO/M, which is shown in the Raman peak position map in Fig. 4e. Furthermore, the full width at half maximum (FWHM) of the E^1_{2g} peak of M/rGO/M broader than that of other regions (Fig. 4f). This indicates that interfacial strain is generated more on the M/rGO/M than on the M/rGO and rGO/M[31,32]. In contrast, the blue shift of A_{1g} on M/rGO and rGO/M is larger than the shift observed in M/rGO/M, which is confirmed in the Raman map shown in Fig. 4g. The FWHM of the A_{1g} peak of M/rGO/M slightly broader than that of other regions (Fig. 4h). This means that the van der Waals (vdW) interlayer interaction between the MoS_2 and rGO on M/rGO and rGO/M is stronger than that of M/rGO/M[31]. According to the previous results, the blue shift of A_{1g} of MoS_2 can originate from the p-doping effect by the functional group of GO[12,33]. The A_{1g} peak appeared to be more strongly shifted as the amount of GO functional groups increased[12]. In this study, rGO was prepared with GO by thermal annealing. Thus, most functional groups of GO were removed and only a small amount of the functional group remained on the surface[25]. In addition, we confirmed that the A_{1g} mode of stacked MoS_2 with rGO was further shifted compared to stacked MoS_2 with GO (see SI, Fig. S9). This means that p-doping of MoS_2 by rGO has a negligible effect on the shift of the A_{1g} peak observed in our stacked MoS_2 with rGO. Therefore, it is concluded that the stacked MoS_2 with rGO spacer is in close contact with vdW interaction between MoS_2 and rGO. We suggest that the rGO can serve as a spacer to decouple the top and bottom MoS_2 and retain the direct band gap of MoS_2.

Conclusions

In conclusion, we successfully fabricated stacked bilayer MoS_2 with rGO spacer. We observed that the decreased PL intensity in the stacked MoS_2 layers without spacer because of bilayer properties. Meanwhile, when the rGO is used as a spacer in between MoS_2 sheets, PL intensity shows sum up of PL from two individual MoS_2 sheets. It clearly indicates that rGO is a suitable material to decouple the top and bottom MoS_2 and retain the direct band gap of MoS_2. In the Raman results, we observed the vdW interaction and the strain effect between the MoS_2 and

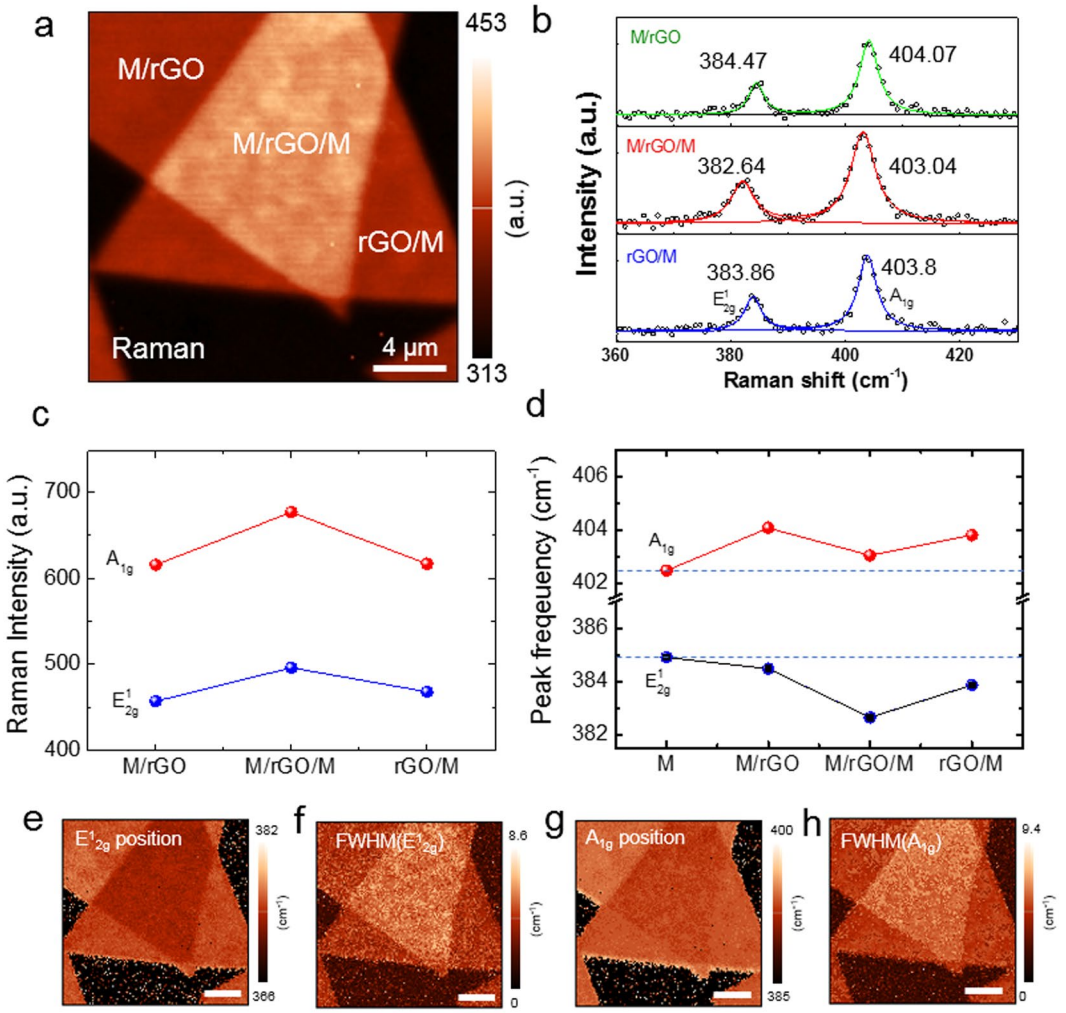

Figure 4. (a) Raman intensity map of the stacked MoS_2 with rGO. (**b**) Local Raman spectra of various position of the stacked MoS_2 with rGO. (**c**) Raman intensity and (**d**) peak position of the E^1_{2g} and A_{1g} of the various position of stacked MoS_2 with rGO. (**e**) Peak position and FWHM map of E^1_{2g} (**f**) peak position and FWHM map of the A_{1g} of the sample.

rGO layers. We expect that these results will provide a fundamental understanding of the interlayer interaction of stacked 2D materials and enable further development of stacked MoS_2-based devices.

Methods

Conventional wet transfer method. Poly(methyl methacrylate) (PMMA) (Micro Chem, 4 wt% in chlorobenzene) was coated onto monolayer MoS_2 grown on a SiO_2/Si substrate to serve as a supporting layer for the transfer process. After being coated with PMMA, the sample was floated on a 1 M potassium hydroxide (KOH) solution at 80 °C to remove the SiO_2 layer. Subsequently, only monolayer MoS_2 with PMMA remained on the KOH solution. The remaining PMMA/MoS_2 was washed with DI water to remove any residual KOH etchant. The washed PMMA/MoS_2 was transferred to the SiO_2/Si substrate. After the drying process was complete, the PMMA was removed using acetone.

Preparation of the GO. GO was synthesized from natural graphite (Alfa Aesar, 99.999% purity, 200 mesh) by modified Hummers' method. First, 5 g of graphite powder and 350 mL of 10 M Sulfuric acid (H_2SO_4) were blended. $KMnO_4$ (15 g) was slowly added over approximately an 1 h. Stirring was continued for 2 h in a cooled water bath. The mixture was strongly stirred for 3 days at room temperature. Deionized water was added and stirring for 10 min. The mixture was stirred for 2 h at room temperature after the addition of an aqueous solution of H_2O_2 (30 wt%). Aqueous solution of HCl (35 wt%) was then added and stirred for 30 min at room temperature. After the supernatant solution was decanted, deionized water was slowly added and stirred for 30 min. The GO solution 1 g/l in water was sonicated for 1 h to exfoliate the GO sheets. To obtain dispersed GO, centrifugation at 10,000 rpm was performed for 1 h, and the supernatant solution was decanted.

Characterization Methods. PL spectra were obtained using a confocal PL spectrometer equipped with an objective lens with high numerical aperture of 0.7 and a diode-pumped solid-state laser (532 nm). Confocal

Raman spectroscopy was conducted using a commercial multifunctional microscope (NTEGRA, NT-MDT). The atomic force microscopy (AFM) topography image and photothermal induced infrared resonance (PTIR) absorption of the sample was obtained using a commercial Nano-IR system (Anasys Instruments).

References

1. Wang, Q. H., Kalantar-Zadeh, K., Kis, A., Coleman, J. N. & Strano, M. S. Electronics and optoelectronics of two-dimensional transition metal dichalcogenides. *Nat. Nanotechnol.* **7**, 699 (2012).
2. Zhao, W. *et al*. Evolution of Electronic Structure in Atomically Thin Sheets of WS_2 and WSe_2. *ACS Nano* **7**, 791–797 (2013).
3. Nayak, P. K., Yeh, C.-H., Chen, Y.-C. & Chiu, P.-W. Layer-Dependent Optical Conductivity in Atomic Thin WS_2 by Reflection Contrast Spectroscopy. *ACS Appl. Mater. Interfaces* **6**, 16020–16026 (2014).
4. Mak, K. F., Lee, C., Hone, J., Shan, J. & Heinz, T. F. Atomically Thin MoS_2 A New Direct-Gap Semiconductor. *Phys.Rev.Lett.* **105**, 136805 (2010).
5. Splendiani, A. *et al*. Emerging Photoluminescence in Monolayer MoS_2. *Nano Letters* **10**, 1271–1275 (2010).
6. Baugher, B. W. H., Churchill, H. O. H., Yang, Y. & Jarillo-Herrero, P. Optoelectronic devices based on electrically tunable p–n diodes in a monolayer dichalcogenide. *Nat. Nanotechnol.* **9**, 262 (2014).
7. Yin, Z. *et al*. Single-Layer MoS_2 Phototransistors. *ACS Nano* **6**, 74–80 (2012).
8. Lopez-Sanchez, O., Lembke, D., Kayci, M., Radenovic, A. & Kis, A. Ultrasensitive photodetectors based on monolayer MoS_2. *Nat. Nanotechnol.* **8**, 497 (2013).
9. Yin, Z. *et al*. Preparation of MoS_2–MoO_3 Hybrid Nanomaterials for Light-Emitting Diodes. *Angew. Chem. Int. Ed.* **53**, 12560–12565 (2014).
10. Tsai, M.-L. *et al*. Monolayer MoS_2 Heterojunction Solar Cells. *ACS Nano* **8**, 8317–8322 (2014).
11. Ming-Wei, L. *et al*. Thickness-dependent charge transport in few-layer MoS_2 field-effect transistors. *Nanotechnology* **27**, 165203 (2016).
12. Oh, H. M. *et al*. Modulating Electronic Properties of Monolayer MoS_2 via Electron-Withdrawing Functional Groups of Graphene Oxide. *ACS Nano* **10**, 10446–10453 (2016).
13. Castellanos-Gomez, A. *et al*. Local Strain Engineering in Atomically Thin MoS_2. *Nano Lett.* **13**, 5361–5366 (2013).
14. Nan, H. *et al*. Strong Photoluminescence Enhancement of MoS_2 through Defect Engineering and Oxygen Bonding. *ACS Nano* **8**, 5738–5745 (2014).
15. Joo, P. *et al*. Functional Polyelectrolyte Nanospaced MoS_2 Multilayers for Enhanced Photoluminescence. *Nano Lett.* **14**, 6456–6462 (2014).
16. Latini, S., Winther, K. T., Olsen, T. & Thygesen, K. S. Interlayer Excitons and Band Alignment in MoS_2/hBN/WSe_2 van der Waals Heterostructures. *Nano Lett.* **17**, 938–945 (2017).
17. Yifeng, C. & Su Ying, Q. Tunable bright interlayer excitons in few-layer black phosphorus based van der Waals heterostructures. *2D Mater.* **5**, 045031 (2018).
18. Srivastava, A. & Fahad, M. S. Vertical MoS_2/hBN/MoS_2 interlayer tunneling field effect transistor. *Solid State Electron* **126**, 96–103 (2016).
19. Gao, J., Liu, C., Miao, L., Wang, X. & Chen, Y. Free-Standing Reduced Graphene Oxide Paper with High Electrical Conductivity. *J. Electron. Mater.* **45**, 1290–1295 (2016).
20. Li, H. *et al*. From Bulk to Monolayer MoS2: Evolution of Raman Scattering. *Adv. Funct. Mater.* **22**, 1385–1390 (2012).
21. Huang, S. *et al*. Probing the Interlayer Coupling of Twisted Bilayer MoS_2 Using Photoluminescence Spectroscopy. *Nano Lett.* **14**, 5500–5508 (2014).
22. Eda, G. *et al*. Photoluminescence from Chemically Exfoliated MoS_2. *Nano Lett.* **11**, 5111–5116 (2011).
23. Katzenmeyer, A. M., Aksyuk, V. & Centrone, A. Nanoscale Infrared Spectroscopy: Improving the Spectral Range of the Photothermal Induced Resonance Technique. *Anal. Chem.* **85**, 1972–1979 (2013).
24. Filimon, M. *et al*. Smart polymer surfaces: mapping chemical landscapes on the nanometre scale. *Soft Matter* **6**, 3764–3768 (2010).
25. Choi, W., Shehzad, M. A., Park, S. & Seo, Y. Influence of removing PMMA residues on surface of CVD graphene using a contact-mode atomic force microscope. *RSC Adv.* **7**, 6943–6949 (2017).
26. English, C. D., Shine, G., Dorgan, V. E., Saraswat, K. C. & Pop, E. Improved Contacts to MoS_2 Transistors by Ultra-High Vacuum Metal Deposition. *Nano Lett.* **16**, 3824–3830 (2016).
27. Yuan, L. *et al*. A reliable way of mechanical exfoliation of large scale two dimensional materials with high quality. *AIP Adv.* **6**, 125201 (2016).
28. Tan, H. *et al*. Doping Graphene Transistors Using Vertical Stacked Monolayer WS_2 Heterostructures Grown by Chemical Vapor Deposition. *ACS Appl. Mater. Interfaces* **8**, 1644–1652 (2016).
29. Tu, N. D. K., Choi, J., Park, C. R. & Kim, H. Remarkable Conversion Between n- and p-Type Reduced Graphene Oxide on Varying the Thermal Annealing Temperature. *Chem. Mater.* **27**, 7362–7369 (2015).
30. Phan, D.-T. & Chung, G.-S. P–n junction characteristics of graphene oxide and reduced graphene oxide on n-type Si(111). *J. Phys. Chem. Solids* **74**, 1509–1514 (2013).
31. Zhou, K.-G. *et al*. Raman Modes of MoS_2 Used as Fingerprint of van der Waals Interactions in 2-D Crystal-Based Heterostructures. *ACS Nano* **8**, 9914–9924 (2014).
32. Wang, Y., Cong, C., Qiu, C. & Yu, T. Raman Spectroscopy Study of Lattice Vibration and Crystallographic Orientation of Monolayer MoS_2 under Uniaxial Strain. *Small* **9**, 2857–2861 (2013).
33. Buscema, M., Steele, G. A., van der Zant, H. S. J. & Castellanos-Gomez, A. The effect of the substrate on the Raman and photoluminescence emission of single-layer MoS_2. *Nano Res.* **7**, 561–571 (2014).

Acknowledgements

This work was supported by the IBS-R011-D1 of Korea and the National Research Foundation of Korea (NRF) with a grant funded by the Korean government (MSIP) (2016R1A2B2015581), the Nano Material Technology Development Program (2014M3A7B6020163) of MSIP/NRF, and the Basic Science Research Program through the National Research Foundation of Korea (NRF) funded by the Ministry of Education (NRF-2016R1A6A3A11936024).

Author Contributions

H.M.O. and M.S.J. designed the experiments. H.M.O. and H.K. fabricated the stacked MoS_2 sample conducted the Nano I.R. experiment. H.M.O. performed P.L. and Raman experiments. H.K. performed growth experiments for graphene. H.M.O. and M.S.J. analyzed the results and wrote the manuscript. All authors discussed the results and commented on the manuscript.

Additional Information

Supplementary information accompanies this paper at https://doi.org/10.1038/s41598-019-42446-w.

Competing Interests: The authors declare no competing interests.

Publisher's note: Springer Nature remains neutral with regard to jurisdictional claims in published maps and institutional affiliations.